biomedicines

MDPI

Article

Fibrin, Bone Marrow Cells and Macrophages Interactively Modulate Cardiomyoblast Fate

Inês Borrego [1], Aurélien Frobert [1], Guillaume Ajalbert [1], Jérémy Valentin [1], Cyrielle Kaltenrieder [1], Benoît Fellay [2], Michael Stumpe [3], Stéphane Cook [1,2], Joern Dengjel [3] and Marie-Noëlle Giraud [1,*]

1   Department of EMC, Faculty of Sciences and Medicine, University of Fribourg, 1700 Fribourg, Switzerland; ines.borrego@unifr.ch (I.B.); aurelien.frobert@unifr.ch (A.F.); guillaume.ajalbert@unifr.ch (G.A.); jeremy.valentin@extern.insel.ch (J.V.); cyrielle.kaltenrieder@unifr.ch (C.K.); stephane.cook@h-fr.ch (S.C.)
2   HFR Hôpital Fribourgeois, 1708 Fribourg, Switzerland; benoit.fellay@h-fr.ch
3   Department of Biology, University of Fribourg, 1700 Fribourg, Switzerland; michael.stumpe@unifr.ch (M.S.); joern.dengjel@unifr.ch (J.D.)
*   Correspondence: marie-noelle.giraud@unifr.ch

Abstract: Interactions between macrophages, cardiac cells and the extracellular matrix are crucial for cardiac repair following myocardial infarction (MI). We hypothesized that cell-based treatments might modulate these interactions. After validating that bone marrow cells (BMC) associated with fibrin lowered the infarct extent and improved cardiac function, we interrogated the influence of fibrin, as a biologically active scaffold, on the secretome of BMC and the impact of their association on macrophage fate and cardiomyoblast proliferation. In vitro, BMC were primed with fibrin (F-BMC). RT-PCR and proteomic analyses showed that fibrin profoundly influenced the gene expression and the secretome of BMCs. Consequently, the secretome of F-BMC increased the spreading of cardiomyoblasts and showed an alleviated immunomodulatory capacity. Indeed, the proliferation of anti-inflammatory macrophages was augmented, and the phenotype of pro-inflammatory switched as shown by downregulated *Nos2*, *Il6* and *IL1b* and upregulated *Arg1*, CD163, *Tgfb* and *IL10*. Interestingly, the secretome of F-BMC educated-macrophages stimulated the incorporation of EdU in cardiomyoblasts. In conclusion, our study provides evidence that BMC/fibrin-based treatment improved cardiac structure and function following MI. In vitro proofs-of-concept reveal that the F-BMC secretome increases cardiac cell size and promotes an anti-inflammatory response. Thenceforward, the F-BMC educated macrophages sequentially stimulated cardiac cell proliferation.

Keywords: macrophages; inflammation; secretome; fibrin; cell communication; cell priming

1. Introduction

Macrophages, the hallmark for tissue healing and wound formation, mediate the inflammatory response following myocardial infarction (MI) and contribute to its resolution [1]. Frangogiannis et al. [2] primarily showed that shifting the balance of macrophages from an inflammatory to an anti-inflammatory phenotype is essential for cardiac regeneration. The roles of macrophages are multifaced, and their importance in the regeneration of the neonatal heart has been identified [3], while it remains mostly unrevealed in the adult myocardium. Extremely versatile, macrophages adopt a variety of functional phenotypes depending on signals in their environment ranging from pro-inflammatory to anti-inflammatory and pro-resolution phenotypes [4]. The different subsets of macrophages can be defined by their function, expression of genes, or responsiveness to activating cytokines [5]. Two major types, namely, alternatively- and classically-activated macrophages, are obtained by treatment of unpolarized macrophages, respectively, with interleukin-4 (IL-4) or lipopolysaccharide (LPS) associated with interferon (INF) respectively.

The spatiotemporal interaction of macrophages with the cardiac extracellular matrix (ECM), cardiomyocytes and non-cardiomyocytes are believed to be a key feature in car-

diac repair and regeneration [6–8]. Consequently, manipulating macrophage subsets has become an emerging therapeutic strategy in numerous diseases, including cardiovascular diseases (CVD) [9,10]. Due to their immunomodulatory capacities, cell-based therapies, including bone-marrow cells (BMC), mononuclear cells (MNC) [11], mesenchymal stromal cells (MSC) [12,13], anti-inflammatory macrophages [14] or their secreted extracellular vesicles have gained interest for treating CVD such as MI [12,15,16]. The secretome of these cells, composed of cytokines, growth factors, and extracellular vesicles or exosomes, is accountable for their paracrine effect which improves cardiac structural and functional outcomes accompanied by mobilization and polarization of macrophages [11,17,18]. For instance, Vagnozzi et al. [11] demonstrated that seven days after ischemia/reperfusion (I/R), bone marrow MNC and MSC improved heart function through an acute immune response characterized by the mobilization of CCR2$^+$ or CX3CR1$^+$ macrophages. In addition, Deng et al. [17] promoted anti-inflammatory macrophage polarization with MSC-exosomes and demonstrated amelioration of cardiac damage after MI.

The use of biomaterials combined with cells is recommended for cell-based therapies [19]. The scaffolds foster cell retention and survival. Nevertheless, scaffolds may also modulate macrophage phenotypes depending on their composition and structure [20,21]. Fibrin, a biologically active scaffold, has gained increasing interest in tissue engineering [22]. Its general use interrogates its influence on the fate of cells. In the present study, fibrin combined with unfractionated BMC was administered sub-chronically in a rat model of MI. Beneficial functional outcomes were recorded after four weeks and were associated with a reduced fibrotic scar. In vitro investigations revealed that the secretome of fibrin primed-BMC (F-BMC) specifically activated macrophages with anti-inflammatory and mitogenic properties.

2. Methods

2.1. In Vivo Study

2.1.1. Animals

Animals were purchased from Janvier (Le Genest, France) and received humane care in compliance with the European Convention on Animal Care and agreement with the Swiss Animal Protection Law. The protocol was approved by the cantonal and Swiss Federal Veterinary Office, Switzerland (FR-2016-41; 23 February 2017) and controlled for reduced animal suffering (all animals received, post-surgery, subcutaneous injection of 0.1 mg kg/L Temgesic).

2.1.2. Bone-Marrow Derived Cells Isolation BMCs and Characterization

BMCs were collected from femurs and tibias of adult rats, flushed with sterile phosphate-buffered saline (PBS; Carl Roth GmbH, Karlsruhe, Germany), incubated in red blood cell lysis buffer (Sigma, Welwyn Garden City, UK) and cultured in Iscove's Modified Dulbecco's Medium (IMDM, Pan Biotech, Aidenbach, Germany) supplemented with 20% Fetal Bovine Serum (FBS, Biochrom AG, Berlin, Germany), 100 IU mL^{-1} penicillin and 100 mg mL^{-1} streptomycin (Corning, Corning, NY, USA). The initial culture medium was changed at passage 1 to Dulbecco's Modified Eagle's Medium–high glucose (DMEM, Sigma–Aldrich, Schaffhausen, Switzerland), with 10% FBS, 100 IU mL^{-1} penicillin and 100 mg mL^{-1} streptomycin. Cells were cultured under aseptic conditions using sterile and RNAse/DNAse free tissue culture-treated plastic ware (Corning, NY, USA) at 37 °C and 5% CO$_2$ in a humidified incubator (Model CB160, Binder, Tuttlingen, Germany). The medium was replaced every two days, and upon 80% confluence, cells were trypsinized, pooled, and subcultured until passage 2. In order to preserve the different populations of the BMCs, cells were collected at passage 2, and no other selection was performed.

For in vivo study, each pool was obtained from 10 male Lewis rats (mean weight of 150 g). For the in vitro study, each pool of BMCs was prepared from 3 male Lewis rats (mean weight of 150 g).

2.1.3. Myocardial Infarction Model

A total of 51 female Lewis rats (mean weight of 200–220 g) were included in the study: following a permanent left anterior descending (LAD) coronary ligation. All surgical interventions were performed under isoflurane and oxygen (5% for induction and 2.5% for maintenance), animals were placed on a warming pad at 37 °C to avoid hypothermia during anaesthesia and ventilated with a 14-G IV cannula at 70–90 cycles per minute (Harvard Inspira Apparatus, Inc.; Holliston, MA, USA). Anaesthetized and ventilated as described. For surgical induction of MI, the proximal left anterior descending (LAD) coronary artery ligation was accessed through a left thoracotomy between the fourth and fifth intercostal space and was permanently ligated (7/0 polypropylene suture, Ethicon, Inc.; Somerville, MA, USA) [23]. Four animals died during or a few days post MI induction. Blood samples were collected 24 h post-MI from the caudal tail artery in the anaesthetized rats, and plasma was isolated using BD Vacutainer® Cell Preparation Tube (Becton Dickinson, Franklin Lakes, NJ, USA) with sodium heparin following manufacturer's instructions. The plasma fraction was immediately frozen and stored at −80 °C. After thawing the samples, the plasma cardiac troponin T (cTnT) level was analyzed on a System Roche Hitachi Cobas (Roche Diagnostics, Basel, Switzerland) [24]. The criterium for selecting the animals was a cTnT level > 900 ng/L [24], resulting in the exclusion of four animals. The mean plasmatic cTnT level was 3028 ± 956 ng/L. Two weeks after MI induction, cardiac function was measured by high-resolution echocardiography; reduced cardiac function assessed after two weeks significantly decreased from 70 ± 2% to 47 ± 8%.

2.1.4. Epicardial Treatment

Two weeks post LAD ligation, 43 rats underwent a second left thoracotomy between the fifth and sixth intercostal space under general anaesthesia [23]. Animals were allocated to the treated or untreated group and received either a sham operation (untreated, *n* = 23) or epicardial implantation on the infarcted myocardium of an association of fibrin (Tisseel®, Baxter Healthcare Pty Ltd., Deerfield, IL, USA) and 2 million BMC (*n* = 20). One animal from the latest group died 11 weeks post-treatment.

2.1.5. High-Resolution Echocardiography

To assess the cardiac function, high-resolution echocardiography was performed with Vevo 3100 imaging system (VisualSonics, Toronto, ON, Canada) equipped with a 21 MHz linear-array transducer (MX250, VisualSonics, Fujifilm, Toronto, ON, Canada). Echocardiograms were recorded at day 0, then at two weeks post-MI (pre-treatment) as well as four- and twelve-weeks post-treatment (post-treatment) in a blinded manner. Each animal was anaesthetized, ventilated and placed on a heating table in a supine position with the extremities fixed with four electrocardiography leads. The chest was shaved and further cleaned with a chemical hair remover for ultrasound attenuation. Warmed Aquasonic gel EcoGel 100 (Eco-Med Pharmaceutical Inc., Toronto, ON, Canada) was applied to the thorax surface to optimize visibility of the cardiac chambers. A rectal probe was placed to control body temperature during the process. The ejection fraction (EF), systolic and diastolic volumes were determined based on parasternal long-axis B-mode image analysis. Left ventricle thickness and fractional shortening (FS), were estimated based on the parasternal long-axis M-mode image analysis. All parameters were calculated with the VevoLab® software (VisualSonics, Toronto, ON, Canada).

2.1.6. Histological Analysis

The heart was harvested, and cross-sections of 2 mm thickness from the base to the apex were obtained for systematic sampling. Each section was embedded in paraffin using a standard histological procedure. The paraffin blocks were sectioned at 5-μm intervals with a manual microtome Shandon Finesse 325 (Thermo Fisher, Waltham, MA, USA) and stained with Masson–Goldner trichrome staining. The slices were successively incubated in Mayer's hematoxylin (Merck AG; Zug, Switzerland), acid fuchsin-ponceau

(Sigma–Aldrich; Buchs, Switzerland), phosphomolybdic acid orange G (Merck AG; Zug Switzerland and Sigma–Aldrich; Buchs, Switzerland), and Lichtgrün (Sigma–Aldrich; Buchs, Switzerland) solutions. The samples were dehydrated with an ascending ethanol series and mounted with Eukitt (EM Sciences; Hatfield, PA, USA). Images were acquired with a stereomicroscope Nikon SMXZ800 mounted with a Nikon 1 camera (Nikon; Tokyo, Japan). Bersoft Image Analysis software (Bersoft Technology and Software; Lunenburg, NS, Canada) was used to measure the scar thickness of the infarct, septum thickness, left ventricle (LV) cavity area, infarct area, and LV tissue area. The infarct expansion index (EI) was calculated as ((LV cavity area/whole LV area)/(infarct thickness/septum thickness)). The measurements were performed on one 5-µm slice from each 2 mm heart section. EI for each heart was the average of 5–6 sections [25].

2.2. In Vitro Studies

2.2.1. Conditioned Medium Preparation

BMCs (0.3×10^6 cells) were cultured in 6-well plates coated with 40 µL fibrin (20 µL thrombin and 20 µL fibrinogen; Tisseel®, Baxter Healthcare Pty Ltd., Deerfield, IL, USA) (F-BMC) or in an uncoated plate (BMC). The ratio cell/fibrin was optimized for low cell mortality (<3% when measured with propidium iodine). Fibrin conditioned medium was obtained after 48 h from a plate coated with 40 µL fibrin. Cd-medium were collected and centrifuged for 5 min at 1200 rpm, immediately used or stored at −80 °C for proteomic analysis.

2.2.2. MS-Based Proteomics

Cd-medium was concentrated by ultrafiltration using vivaspin columns (10 kDa MWCO). Samples were heated in SDS-PAGE loading buffer, reduced with 1 mM DTT for 10 min at 75 °C and alkylated using 5.5 mM iodoacetamide for 10 min at RT. Protein mixtures were separated on 4–12% gradient gels (Nupage, Thermo Fisher). Gel lanes were cut into 6 slices, and proteins therein were in-gel digested with trypsin (Promega, Dübendorf, Switzerland), and resulting peptide mixtures were processed on STAGE tips and analyzed by LC-MS/MS.

Mass spectrometric measurements were performed on a QExactive Plus mass spectrometer (Thermo Scientific) coupled to an EasyLC 1000 nanoflow-HPLC. HPLC-column tips (fused silica) with 75 µm inner diameter were self-packed with Reprosil–Pur 120 C18-AQ, 1.9 µm (Dr Maisch GmbH, Ammerbuch, Germany) to a length of 20 cm. Samples were applied directly onto the column without a pre-column. A gradient of A (0.1% formic acid in water) and B (0.1% formic acid in 80% acetonitrile in water) with increasing organic proportion was used for peptide separation (loading of the sample with 0% B; separation ramp: from 5–30% B within 85 min). The flow rate was 250 nL/min and 600 nL/min for sample application. The mass spectrometer was operated in the data-dependent mode and switched automatically between MS (max. of 1×10^6 ions) and MS/MS. Each MS scan was followed by a maximum of ten MS/MS scans using a normalized collision energy of 25% and a target value of 1000. Parent ions with a charge state from z = 1 and unassigned charge states were excluded for fragmentation. The mass range for MS was m/z = 370 − 1750. The resolution for MS was set to 70,000 and for MS/MS for 17,500. MS parameters were as follows: spray voltage 2.3 kV; no sheath and auxiliary gas flow; ion–transfer tube temperature 250 °C.

MS raw data files were uploaded into the MaxQuant software version 1.6.10.43 for peak detection, generation of peak lists of mass error-corrected peptides, and for database searches (PMID 19029910). A full-length UniProt rat database containing additional common contaminants such as keratins and enzymes used for in-gel digestion (based on UniProt rat FASTA version May 2019) was used as reference. Carbamidomethylcysteine was set as a fixed modification, and protein amino-terminal acetylation and oxidation of methionine were set as variable modifications. LFQ was chosen as the quantitation mode. Three missed cleavages were allowed, enzyme specificity was trypsin/P, and the MS/MS tolerance was set to 20 ppm. The average mass precision of identified peptides was, in

general, less than 1 ppm after recalibration. Peptide lists were further used by MaxQuant to identify and relatively quantify proteins using the following parameters: peptide and protein false discovery rates, based on a forward-reverse database, were set to 0.01, minimum peptide length was set to 7, the minimum number of peptides for identification and quantitation of proteins was set to one which must be unique, minimum ratio count was set to two, and identified proteins were again quantified. The interleukins were not in the detection range of the actual proteomic protocol.

2.2.3. Macrophage Isolation, Differentiation and Priming with Condition Media

Monocytes were isolated from the bone marrow of seven different pools of 3 male Lewis rats (mean weight of 150 g) (Janvier, Le Genest-Saint-Isle, France) and cultured during seven days in DMEM medium, 10% FBS, 100 IU mL^{-1} penicillin and 100 mg mL^{-1} streptomycin, supplemented with 50 ng mL^{-1} of macrophage colony-stimulating factor (M-CSF, Peprotech, London, UK) (Murray 2014). Cells were washed with PBS and stimulated with either LPS (50 ng mL^{-1}; Sigma–Aldrich; Buchs, Switzerland) and IFN (10 ng mL^{-1}; rat recombinant; Peprotech, London, UK) to trigger their differentiation towards a pro-inflammatory phenotype $M_{(LPS,IFN)}$ or IL-4 (20 ng mL^{-1}, rat recombinant; Peprotech, London, UK) to obtain anti-inflammatory macrophages, $M_{(IL-4)}$ or kept untreated for unpolarized macrophages ($M_{(-)}$)(adapted from [26]). $M_{(-)}$, $M_{(LPS,INF)}$ and $M_{(IL-4)}$ were further cultured, during 48 h, with F-BMC, BMC or fibrin conditioned media. Culture with DMEM 10% medium served as control. The differentiation of the macrophages was validated by surface markers and expression profiles accessed by immunostaining and RT-PCR, respectively.

2.2.4. Enzyme-Linked Immunosorbent Assay (ELISA)

F-BMC, BMC or fibrin were cultured in the control medium (DMEM, 10% FBS, 1% P/S). After 48 h, the media were harvested and centrifuged. The macrophages were cultured for 48 h, with the conditioned media of F-BMC, BMC or substrate. Then, macrophages were washed with PBS and cultured with standard medium (DMEM, 10% FBS, 1% P/S). After 48 h, the cytokines were quantified in the medium harvested from the educated macrophages. ELISA kits (IL-1β (ab100767; Abcam, Cambridge, UK), IL-6 (ab119548; Abcam, Cambridge, UK), TNF-alfa (ab46070; Abcam, Cambridge, UK)) were used according to the manufacturer's instructions and were estimated as pg/mL. Absorbance was read on a Tecan Infinite 200 PRO Microplate Reader (Tecan Group, Mennedorf, Switzerland).

2.2.5. Real-Time Polymerase Chain Reaction

RNA was isolated from BMC cultured with or without fibrin and from the different macrophage phenotypes previously cultured with BMC, F-BMC, fibrin conditioned media or with standard growth medium, using the Trizol Reagent (Molecular Research Center, Inc., Cincinnati, OH, USA) according to the manufacturer's instructions. RNA was reverse transcribed to generate complementary DNA, using GoScript Reverse Transcription Mix™ (Promega, Madison, WI, USA) according to the manufacturer. Two-step quantitative Real Time-PCR was performed to measure mRNA expression using a StepOne SYBR System (Thermo Fisher Scientific, Basel, Switzerland) with GoTaq® qPCR Master Mix (Promega, Madison, WI, USA) and acquired with StepOne software v.2.3. (Thermo Fisher Scientific, Switzerland). mRNA expression was assessed using primers as presented in Supplementary Table S2. The mRNA expression levels of all genes were quantified by normalizing to the geometric mean of the reference genes *GAPDH* and *beta-actin* and using the relative quantification of gene expression calculated by the $2^{-\Delta\Delta Ct}$ approximation method.

2.2.6. H9C2 Rat Cardiomyoblasts

H9C2 rat cardiomyoblasts (Sigma–Aldrich; Buchs, Switzerland) were expanded in Dulbecco's Modified Eagle's Medium—high glucose (DMEM, Sigma–Aldrich, Switzerland), with 10% FBS, 100 IU mL^{-1} penicillin and 100 mg mL^{-1} streptomycin. Cardiomyoblasts

were further cultured for 48 h with DMEM 10% medium or conditioned media from F-BMC, BMC, fibrin, or macrophages. Additionally, H9C2 were cultured with F-BMC, fibrin, or BMC educated macrophages. To obtain the double conditioned medium, the macrophages were cultured with the fibrin, BMC, or F-BMC conditioned media for 48 h; the educated macrophages condition media were collected, centrifuged and added to the H9C2.

2.2.7. Real-Time Cell Analyzer System (RTCA) and EdU Cell Proliferation Assays

An E-Plate® was seeded with 10,000-cells/well with gold microelectrodes fused to the bottom surface and cultured for 120 h using the instrument xCELLigence Real-Time Cell Analyzer (RTCA; ACEA Biosciences Inc., Penzberg, Germany) according to the manufacturer's instructions. The cell index (CI; impedance measurement correlated with cell proliferation) was recorded for 120 h. CI was plotted against time (hours), and the area under the curve (AUC) was calculated [27].

An EdU Cell Proliferation Kit (Sigma–Aldrich; Buchs, Switzerland) was used according to the manufacturer's instructions. Pictures of stained cells were acquired using a Cytation 5 Cell Imaging Multi-Mode Reader (Biotek, Switzerland), and the percentage of positive EdU cells per field was counted using Gen5 software (Biotek, Switzerland).

2.3. Statistical Analysis

Statistical analyses were performed using statistical software GraphPad Prism, Version 8 (GraphPad Software, San Diego, CA, USA). All values were reported as mean $\pm$ standard deviation (SD). Data distribution was assessed using the Kolmogorov–Smirnov test. For the in vivo study, an unpaired *t*-test was performed. For the in vitro study, one-way ANOVA was performed, followed by a Dunnett's multiple comparisons test or otherwise indicated. Results were considered significant from $p < 0.05$.

3. Results

3.1. In Vivo Study

BMC associated with fibrin restores cardiac function loss and reduces the fibrotic scar in the infarcted heart.

Epicardial implantation of fibrin and BMC was performed two weeks after the induction of MI by LAD ligation in a rat model, and the therapeutic potential was evaluated.

Before the treatment and four weeks post-treatment, functional and structural characteristics were assessed by high-resolution echocardiography. The differences in EF and FS in the treated group were calculated. As shown in Figure 1A, the treated group showed statistically significant EF and FS gains, compared to the untreated group that showed a loss in cardiac function (Figure 1A). It is important to note that the gain in EF and FS showed high inter-individual variability. Indeed, the highest and the lowest EF gain measured were +14% and −8%, respectively, in the treated groups and +3% and −11% in the control group, respectively. Structural adaptations also differed between groups with augmented systolic wall thicknesses and reduced LV volumes in treated animals (Figure 1A).

Furthermore, Masson's trichrome staining was performed four weeks post-treatment (Figure 1B). Calculation of the infarct expansion index demonstrated that the scar was substantially smaller in the treated than in the untreated groups (Figure 1B), indicating that the treatment significantly decreased cardiac fibrosis. Seven animals per group were kept twelve weeks post-treatment. One animal in the treated group died after 11 weeks. Twelve weeks post-treatment, the mean scar expansion index was decreased in treated animals compared to control ones; however, the difference did not reach statistical significance.

Further immunostaining showed that the percentage of CD68 and CD206 macrophages present in the infarcted myocardium and the peri infarcted area after 4 and 12 weeks was similar in all groups (Figure S1).

3.2. In Vitro Study

3.2.1. Unique Characteristics of F-BMC, Including Growth, Gene Expression and Secretion Profile Distinguish Them from BMC

BMC are a heterogeneous population of cells as indicated by markers from the mesenchymal and hematopoietic lineages (Figure S2); the mesenchymal CD90+ cells were most abundant. Fibrin induced a change in the morphology of BMC (Figure 2). While BMC displayed a homogeneous spindle-like shape, F-BMC presented rounded cell morphology. The proliferation of F-BMC was measured by EdU incorporation and revealed a significant reduction compared to BMC (Figure 3A). In addition, cell growth was assessed using a real-time cell analyzer (RTCA), in which microelectrodes measure the electrical impedance of the cell populations assessing both the cell number and cell spreading. Results are presented as the area under the curve (AUC) after 5 days (Figure 3B). The AUC of F-BMC was significantly lower than the AUC of BMC, confirming reduced cell growth and spreading. Taken all together, our data show that fibrin decreased both the proliferation and the spreading of BMC.
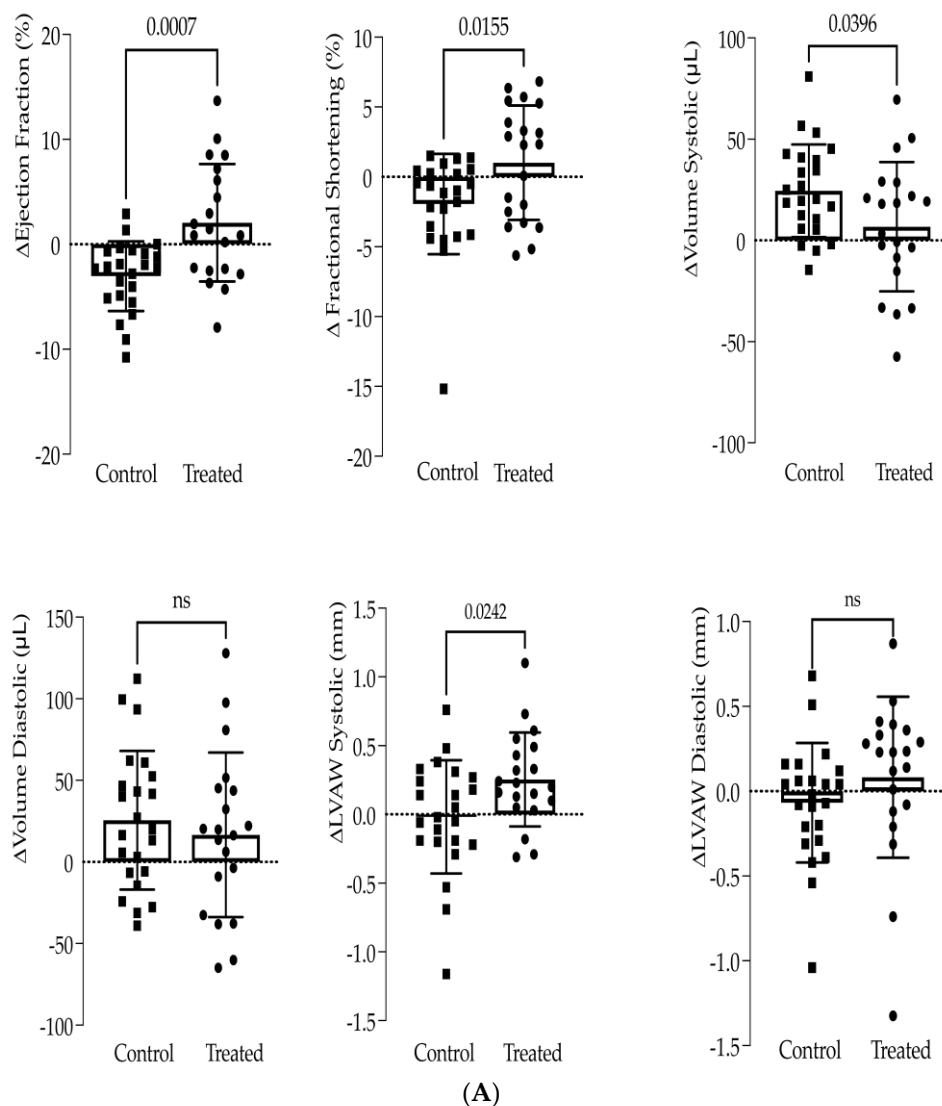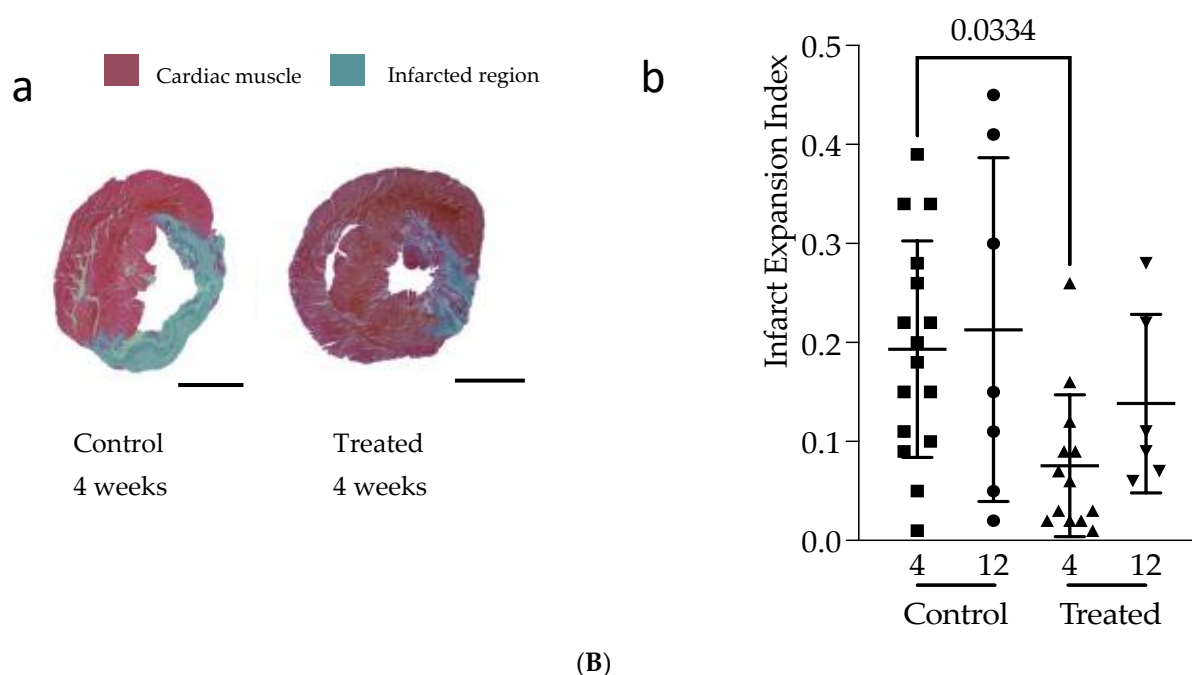

(A)

Figure 1. *Cont.*

(**B**)

Figure 1. (**A**) Fibrin and BMC treatment reduces systolic heart function loss. Cardiac function was assessed by high-resolution echocardiography. The changes (Δ) in ejection fraction, fractional shortening, left ventricle (LV) volumes and LV wall thickness (LVAW) were calculated as the difference between 4 weeks post- and pre-treatment. The control group is untreated (sham) infarcted animals (*n* = 23); the treated group is animals treated with epicardial fibrin and BMC (*n* = 20). (**B**) Fibrin and BMC treatment reduces fibrotic scar. (**a**) Representative Masson–Goldner trichrome stained heart cross-sections from treated and control (sham) animals, 4 weeks post-treatment. The fibrotic scar tissue is in blue; in red is the remote tissue. Scale bars indicate 3 mm. (**b**) Infarct Expansion Index was measured on histologic sections 4 weeks or 12 weeks post-treatment. A total of 5 to 6 cross-sections from systematic sampling of the whole heart were averaged for each animal. Each point represents one animal. The control group is infarcted animals that received sham treatment. The treated group is animals treated with epicardial fibrin and BMC. The values are shown as mean ± SD.
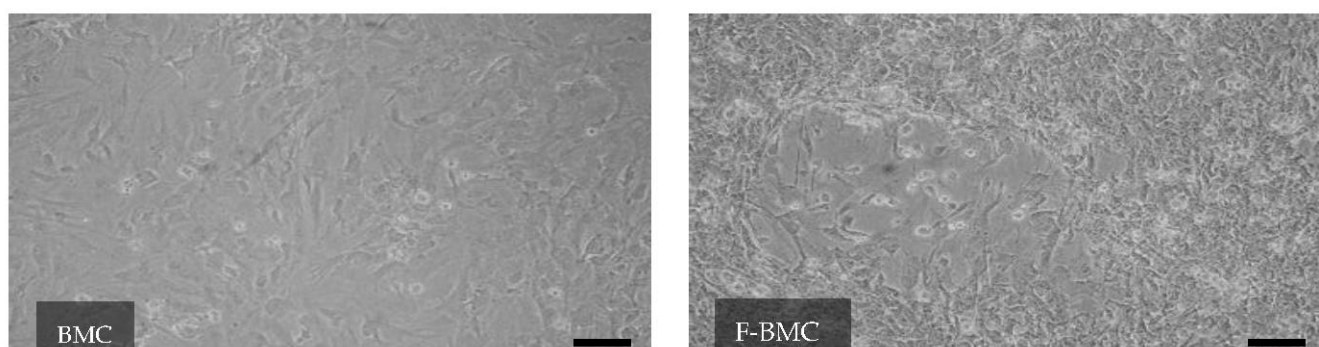

Figure 2. Fibrin modulates the BMC morphology: Representative pictures of BMC cultured with fibrin (F-BMC) or without (BMC) showing a heterogeneous population of cells with different morphology and spreading. Scale bar = 100 μm.

The Conditioned media (Cd-media) of F-BMC and BMC were analyzed by liquid chromatography (LC)-tandem mass spectrometry (MS/MS). In total, 1712 proteins were identified (protein and peptide FDR < 0.01), of which 769 were quantified with a minimum of two replicates out of three per group using label-free quantification based on respective peptide ion currents [28]. Hierarchical clustering of data nicely discriminated the two ex-

perimental groups indicating that Cd-media of F-BMC and BMC differed in their proteomic composition on a global scale (Figure 4A). In total, protein abundances of 339 proteins were significantly altered between the two groups, 185 were significantly upregulated, and 154 were downregulated when comparing F-BMC to BMC (Figure 4B; *t*-test, FDR < 0.05). Upregulated proteins could be linked to metabolic and catabolic processes, inflammation response and ECM remodelling (Figure 4C, Supplemental Table S1; BH FDR < 0.02).
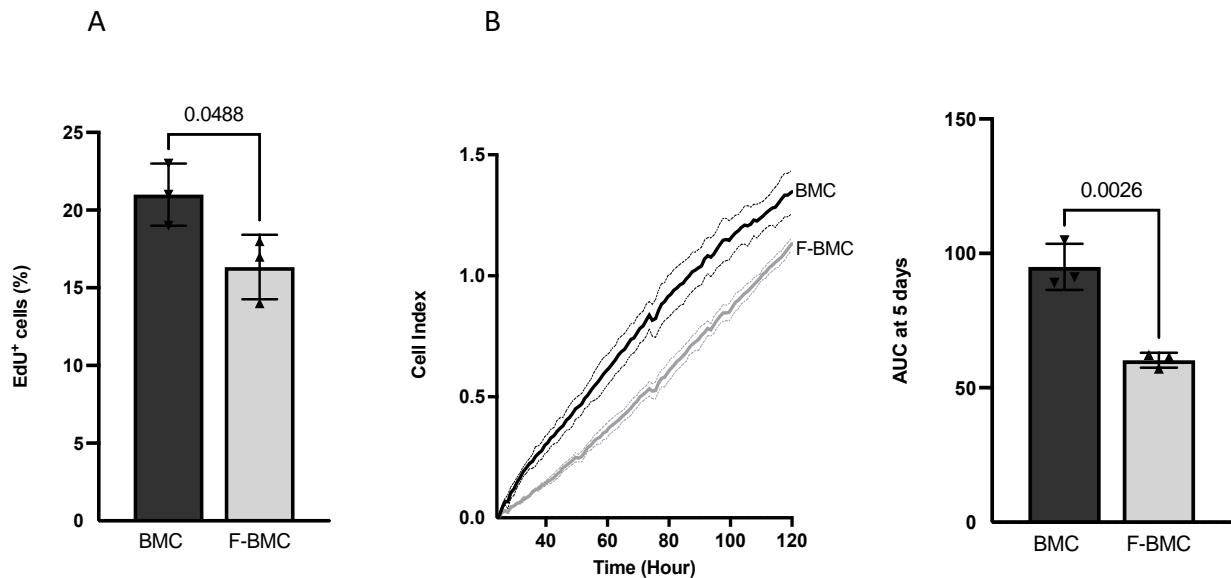

Figure 3. Fibrin modulates BMC proliferation: BMC were cultured with (F-BMC) or without fibrin (BMC). Cell growth was assessed by (**A**) EdU incorporation for 48 h and by (**B**) RTCA: Cell index was measured over 120 h, plotted, and the AUC calculated. The values are shown as mean ± SD; *n* = 3 biologically independent samples of pools of the BMC of 3 rats i.

In complement, RT-PCR was performed using RNA isolated from F-BMC and BMC. Differential expressions of genes involved in inflammation and ECM organization were prioritized (Figure 5). Furthermore, as proteomics did not allow the quantification of interleukin secretions, their expressions were investigated by RT-PCR.

Fibrin priming induced a significant upregulation of *TIMP1* expression and down-regulation of the proteolytic enzymes *MMP3* and *MMP9* (Figure 5). In agreement, the level of protein secretions of TIMP1 and MMP9 exhibited the same significant trends (Supplemental Table S1). *Vcam1*, *Icam* and the inflammation mediators *Nos2* and *Tgfb* were significantly downregulated by fibrin, whereas *Il1ra*, *Il1b*, *IL6*, and *Gmcsf* expression increased. (Figure 5). Concerning *Tnfa*, the gene expression was upregulated; however, the difference in the secretion of TNF-alpha between BMC and F-BMC did not reach statistical significance as shown in the proteomic analysis (Supplemental Table S1). *Ccl2/Mcp1* gene expression and related protein secretion were augmented (Figure 5, Supplemental Table S1). While *Csf1/Mcsf* expression was not statistically changed, the secretion of the protein increased. Chemokines were also significantly modulated by fibrin. *Ccl5/Rantes* expression increased while *Cxcl10* decreased (Figure 5). In parallel, the secretion of CxCL2, CxCL3, CxCL4/PF4, CCL7 and CCL9 were significantly higher in F-BDMC (Supplemental Table S1). Also, proteomic analysis revealed the modulation of proteins such as Osteopontin (ONP/SPP1) and Gremlin1 (GREM1) that were both increased by fibrin (Supplemental Table S1).

Collectively, these results show that fibrin profoundly influenced gene expression and the cell proteome, simultaneously upregulating both pro-and anti-inflammatory mediators.
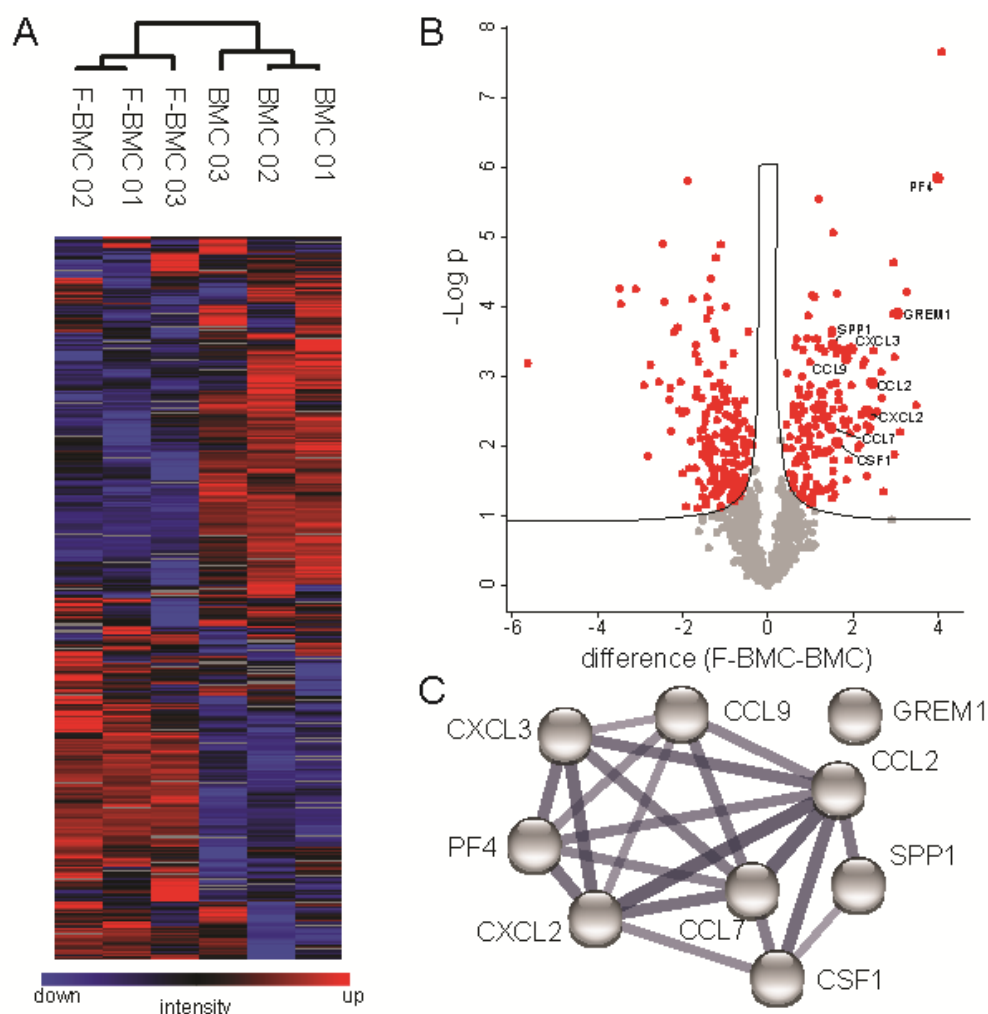
Figure 4. Expression proteomic analyses of BMCs cultured with and without a fibrin-based substrate. (**A**) Hierarchical clustering of protein abundances using log2 transformed and z-normalized LFQ intensities indicates global alterations of CM due to culture conditions. Grey squares indicate proteins not detected in respective samples. (**B**) Volcano plot analysis highlights significantly altered proteins due to culture condition in red (FDR < 0.05). The black line indicates S0 of 0.1. (**C**) Eight cytokines known to interact based on STRING DB are significantly downregulated in BMCs cultured with the fibrin-based substrate [29]. The thickness of edges indicates the confidence of data support.

3.2.2. F-BMC Secretome Promotes the Proliferation of Undifferentiated and Anti-Inflammatory Macrophages

The effects of the secretomes of BMC and F-BMC on macrophage fates were investigated. The proliferation of undifferentiated ($M_{(-)}$), pro-and anti-inflammatory macrophages (respectively, $M_{(LPS, IFN)}$ and $M_{(IL-4)}$) cultured with Cd-media from BMC, F-BMC and fibrin were assayed by EdU incorporation. After 48 h, the percentage of $EdU^+ M_{(-)}$ increased significantly when cultured with Cd-media from both F-BMC and BMC (Figure 6A) relative to the unconditioned medium (control). Cd-medium from fibrin had no significant effect. The proliferation rate of $M_{(LPS, IFN)}$ remained quantitatively low and similar for all conditions (Figure 6B). Compared to control, the proliferation of $M_{(IL-4)}$ was statistically significantly stimulated by the F-BMC secretome. There was no statistically significant difference between BMC and control nor between BMC and F-BMC. Altogether, our results show that F-BMC and BMC modulated the proliferation of $M_{(-)}$ and $M_{(IL-4)}$ macrophages.
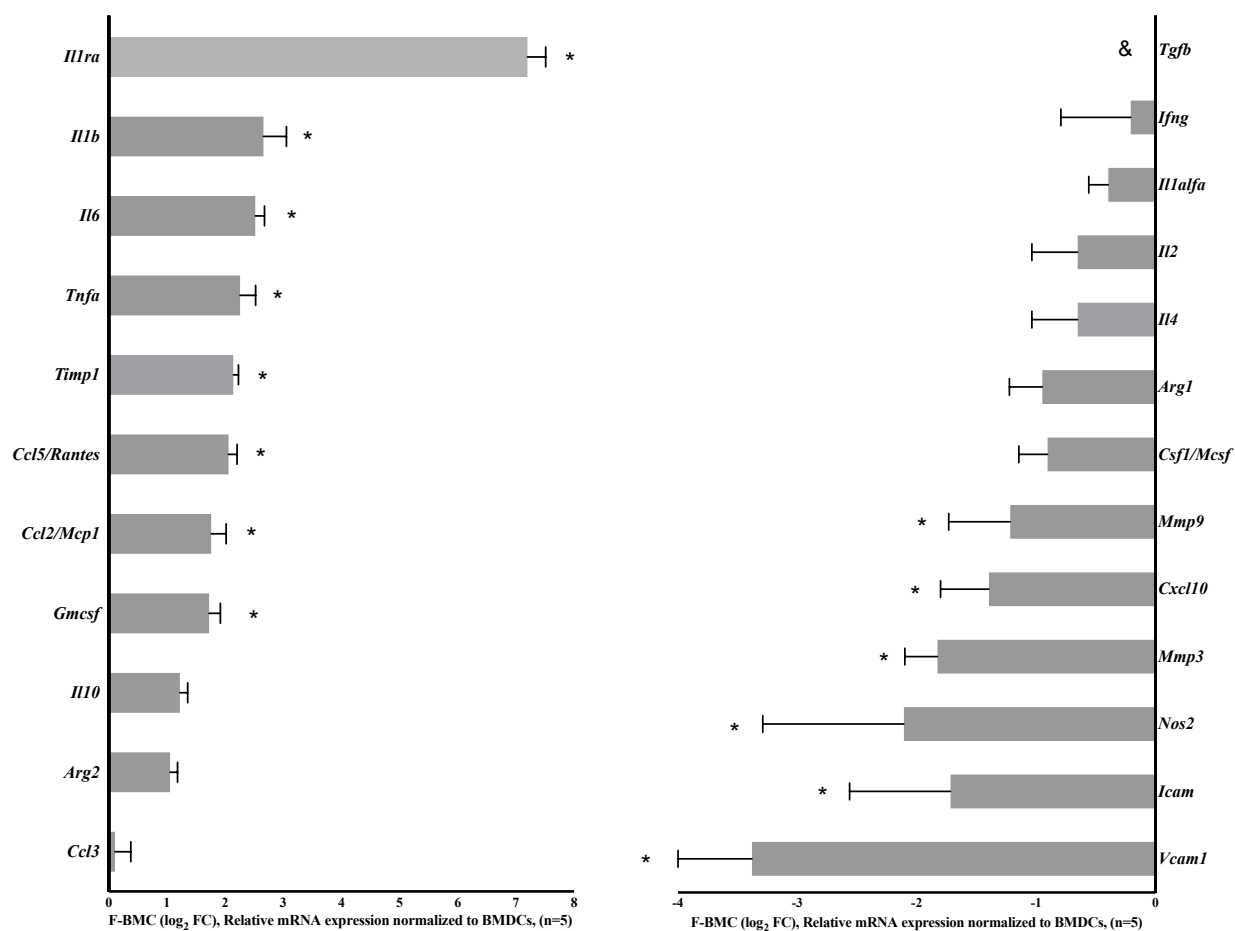
Figure 5. Fibrin modulates BMC gene expression. Real-time PCR measurement of selected genes presented as fold change (FC). *n* = 5 biologically independent samples of cell pools from 3 rats. * $p < 0.05$, shows the statistical significance between differential gene expression of F-BMC related to BMC assessed by one-way ANOVA and Dunnett's test.

3.2.3. F-BMC Secretome Induces a Macrophage Phenotype Switch

RT-PCR was performed using RNA isolated from macrophages cultured with Cd-media from F-BMC (F-BMC educated macrophages) (Figure 7), BMC and fibrin (Figure S3). F-BMC-educated M$_{(-)}$ showed a significantly downregulated expression of pro-inflammatory genes, particularly *Nos2*, *Il6* and *Ccl2/Mcp1*. Anti-inflammatory genes such as *Arg1*, *Tgfb* and *IL-10* were significantly upregulated (Figure 7A). Similar gene regulations were recorded for F-BMC-educated M$_{(LPS,INF)}$ with a significant downregulation of *Il1b* and no change for *Ccl2/Mcp1* (Figure 7B). Remarkably, the anti-inflammatory phenotype of the macrophage M$_{(IL-4)}$ was further stimulated. All tested pro-inflammatory genes were significantly down-regulated, and all studied anti-inflammatory ones were upregulated (Figure 7C).

The expressions of the surface markers of F-BMC-educated macrophages were significantly altered, specifically the markers *Cd206* and *Cd163* related to alternatively activated macrophage phenotypes. *Cd206* was significantly upregulated in M$_{(-)}$ and M$_{(IL-4)}$ (Figure 7A,C), while *Cd163* was significantly upregulated in all macrophages. Further, the classical activated macrophage marker *Cd86* was downregulated in M$_{(IL-4)}$ (Figure 7B). The switch of macrophage plasticity to an anti-inflammatory profile was observed in BMC educated macrophages. The gene expression switch was more prominent for F-BMC educated M$_{(-)}$ and M$_{(LPS, IFN,}$ (Figure S3). Fibrin also showed a different regulatory pattern in M$_{(LPS,INF)}$ and M$_{(-)}$ compared to BMC and F-BMC (Figure S3).
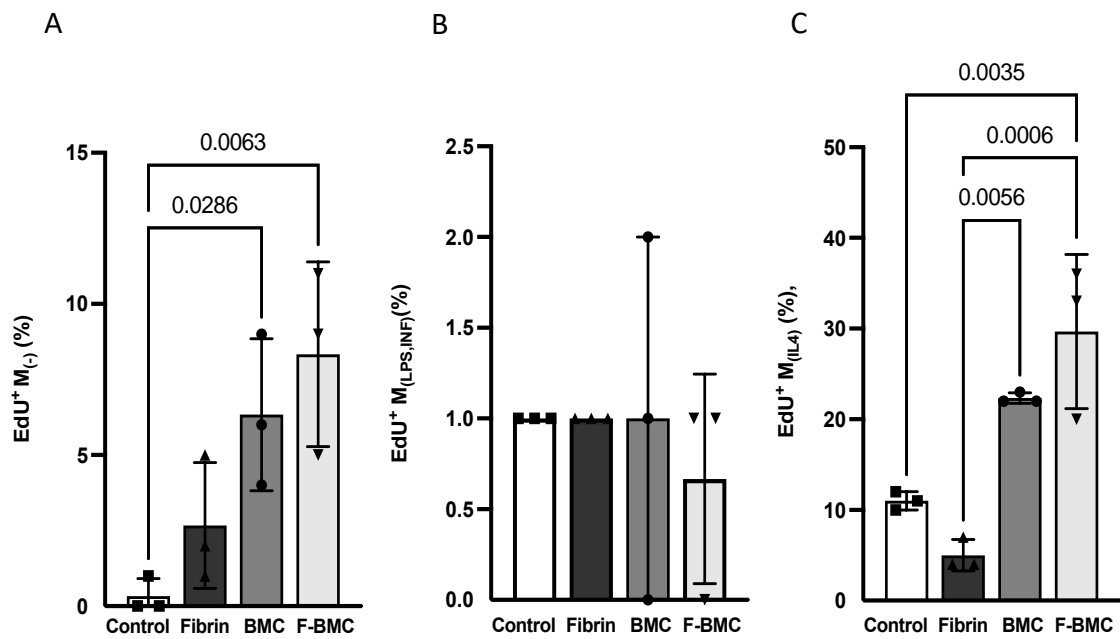
Figure 6. F-BMC and BMC conditioned media modulate macrophage proliferation. The proliferation of the different macrophages phenotypes was assessed by EdU incorporation. (**A**) $M_{(-)}$, (**B**) $M_{(LPS,IFN)}$, and (**C**) $M_{(IL-4)}$ macrophages were cultured with unconditioned medium (Control) or conditioned media from with Fibrin, F-BMC and BMC. The values shown are mean $\pm$ SD. n = 3 biologically independent pools of macrophages from 3 animals, therefore, in total, 9 animals per group.
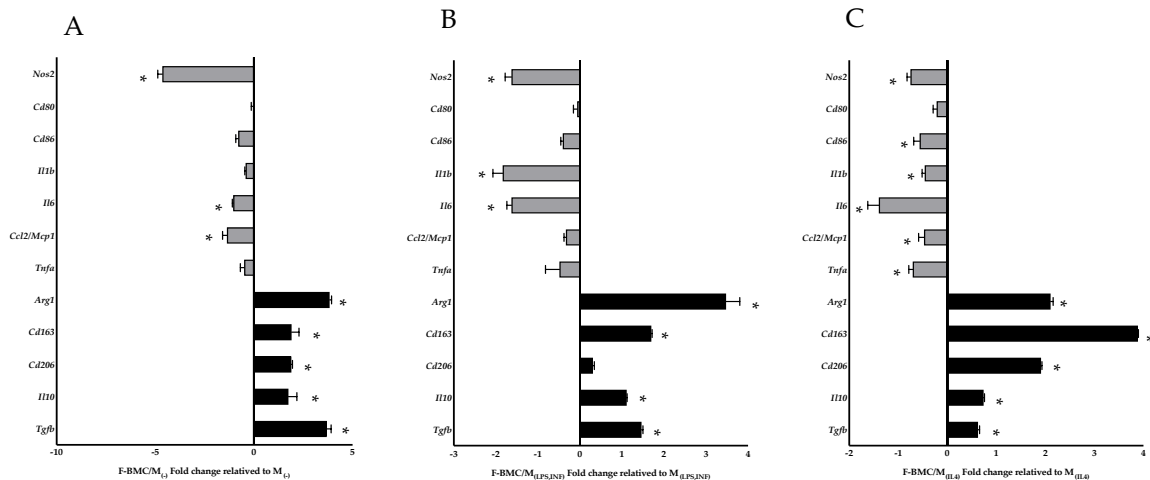

Figure 7. F-BMC conditioned medium modulates the macrophage expression profile. Relative gene expression of pro-inflammatory markers (grey) and anti-inflammatory markers (black) measured in F-BMC educated macrophages: (**A**) $M_{(-)}$, (**B**) $M_{(LPS, IFN)}$ and (**C**) $M_{(IL-4)}$ relative to uneducated ones. The values are shown as mean $\pm$ SD. All n= 3 biologically independent samples were constituted of macrophage pools, each pool was obtained from three animals, therefore, in total, nine animals per group. * $p < 0.05$, shows the statistical significance between differential gene expression of F-BMC educated macrophages and uneducated ones assessed by one-way ANOVA and Dunnett's test.

The levels of IL-1beta, IL-6 and TNF-alpha secreted by F-BMC-educated macrophages were further quantified by enzyme-linked immunosorbent assay (ELISA). Unconditioned medium served as the control. IL-1beta levels were significantly decreased in $M_{(LPS,INF)}$ and $M_{(IL-4)}$ with respective -2.8 and -5.8 fold changes compared to control (Figure 8). IL-6 levels were significantly decreased for $M_{(-)}$, $M_{(LPS,INF)}$ and $M_{(IL-4)}$ with -3.7, -2.8 and -3.0 fold changes, respectively (Figure 8). TNF-alpha secretion was also significantly lower

in $M_{(-)}$ and $M_{(LPS,IFN)}$ with fold changes of -4.0 and -2.8, respectively (Figure 8). The decrease in the secretion of cytokines corroborated the changes in gene expression measured with RT-PCR. Taken all together, the results show that F-BMC-educated macrophages decreased both the expression and the secretion of different proteins related to a pro-inflammatory phenotype.
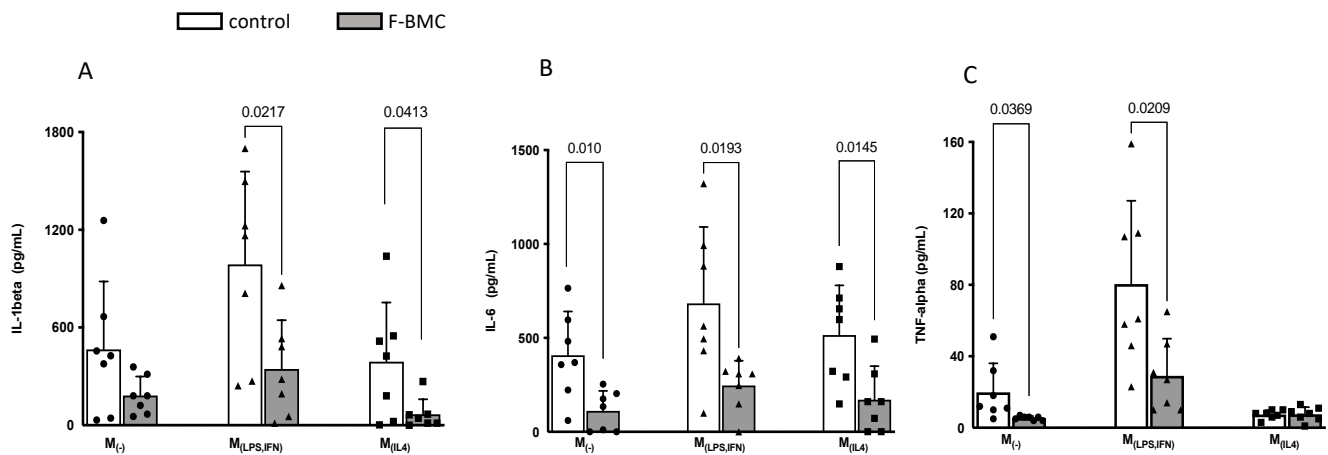

Figure 8. F-BMC conditioned medium modulated the macrophage secretion profile. Cytokine expression levels of (**A**) IL-1 beta, (**B**) IL-6 and (**C**) TNF-α were quantified by ELISA in cell culture supernatants of $M_{(-)}$, $M_{(LPS,IFN)}$, and $M_{(IL-4)}$ educated with F-BMC conditioned medium or unconditioned medium. The values are shown as mean $\pm$ SD. $n = 7$ biologically independent macrophage pools; each pool was obtained from three animals.

3.2.4. F-BMC Secretome Promotes Cardiomyoblast Spreading

Cardiomyoblasts (H9C2) were chosen as a model of proliferative cardiac cells. The proliferation of H9C2 cultured with Cd-media from BMC, F-BMC and fibrin was compared to an unconditioned medium (control) and measured using EdU incorporation. After two days, the percentage of EdU$^+$ H9C2 was significantly higher with F-BMC compared to BMC and Fibrin Cd-media (Figure 9A) and was similar to the control.
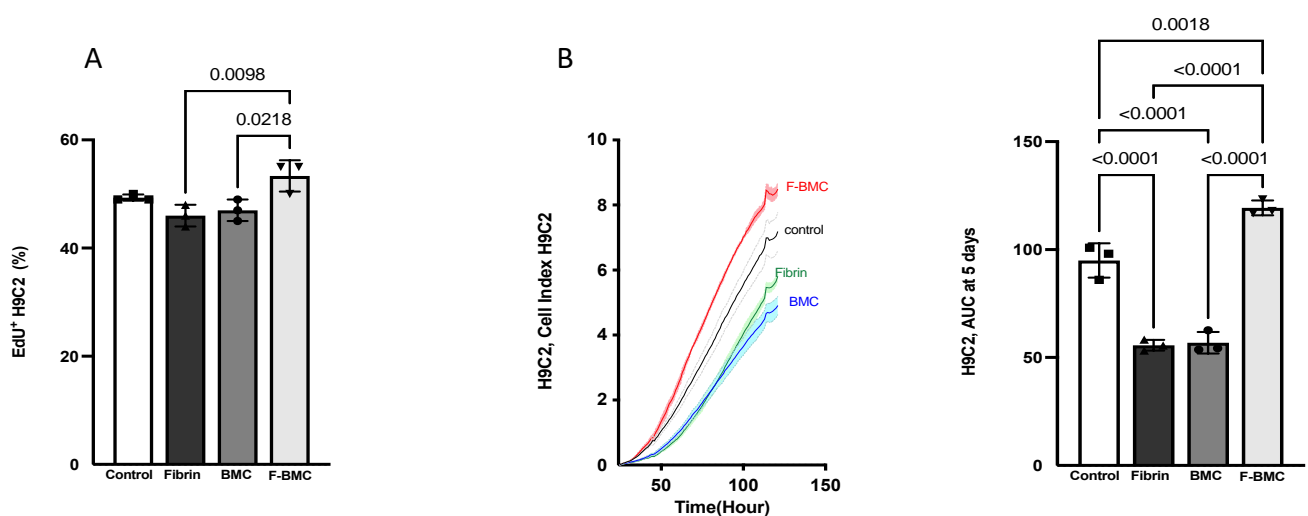

Figure 9. F-BMC, BMC and fibrin secretomes altered cardiomyoblast H9C2 growth. H9C2 were cultured with Cd-media from F-BMC, BMC or fibrin. Standard growth medium served as control. H9C2 growth was assessed by (**A**) EdU incorporation during 48 h and by (**B**) RTCA: Cell index was measured over 120 h, and the AUC was calculated after five days. The values are shown as mean $\pm$ SD; $n = 3$ biologically independent experiments.

In addition, the F-BMC secretome significantly increased the AUC of H9C2, suggesting an increased spreading with or without an increased cell number. The cell index measured by RTCA (Figure 9B) corroborated the proliferation assay. Taken all together, our results suggest that the F-BMC secretome induced an increase in H9C2 spreading and had no effect on cell proliferation when compared to the control condition. In contrast, fibrin and BMC secretomes reduced both H9C2 spreading and proliferation compared to F-BMC.

3.2.5. Alternatively-Activated Macrophages Promote Cardiomyoblast Proliferation

Cd-media obtained from unpolarised and polarised macrophages were used to cul-ture H9C2 (Figure 10). EdU$^+$ cells and AUC were significantly increased for $M_{(IL-4)}$, suggesting that the secretome of alternatively activated macrophages increased the H9C2 proliferation rate. $M_{(-)}$ and $M_{(LPS,INF)}$ did not alter the spreading of H9C2 compared to the control. $M_{(LPS,INF)}$ reduced H9C2 proliferation.
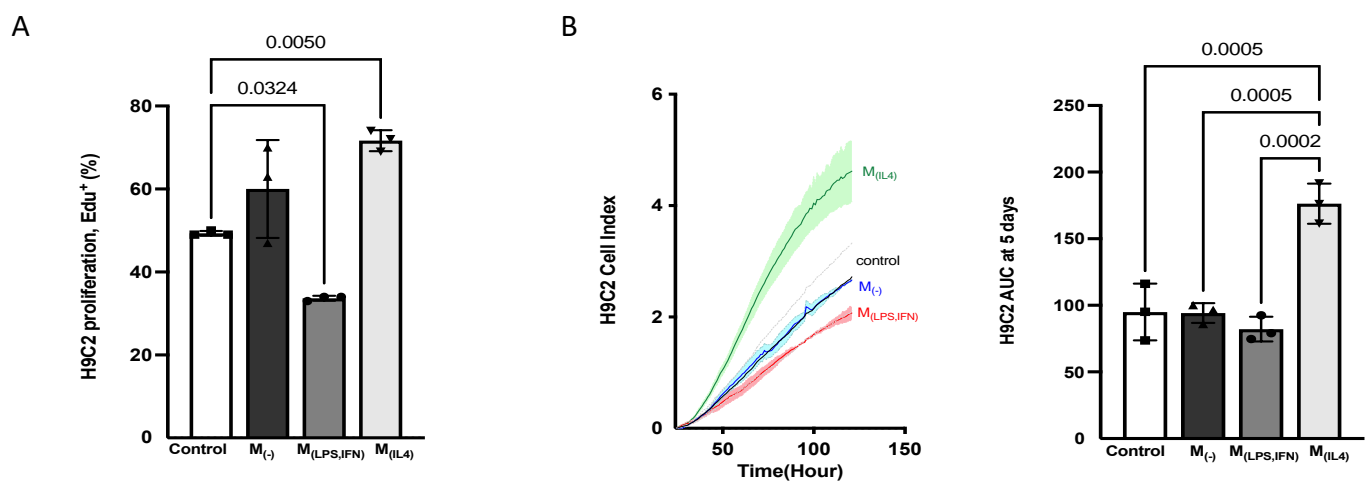

Figure 10. Macrophage secretomes altered the cardiomyoblast H9C2 proliferation rate and spreading. H9C2 were cultured with Cd-media from $M_{(-)}$, $M_{(LPS,IFN)}$ or $M_{(IL-4)}$. Standard growth medium served as control. H9C2 growth was assessed by (**A**) EdU incorporation during 48 h and by (**B**) RTCA: Cell index was measured over 120 h, and the AUC was calculated after five days. The values are shown as mean $\pm$ SD; n = 3 biologically independent experiments.

3.2.6. F-BMC-Educated-Macrophages Demonstrate Paracrine Mitogenic Properties on Cardiac Cells

Educated macrophages were obtained from $M_{(-)}$, $M_{(LPS,IFN)}$ or $M_{(IL-4)}$ macrophages primed with Cd-media from BMC, F-BMC or fibrin. Then, H9C2 were cultured with secretomes from educated or uneducated macrophages (Figure 11). The secretome of F-BMC-educated $M_{(-)}$ (labelled as $M_{(-)}$/F-BMC) modulated the growth of H9C2 as shown by the significant increase of the percentage of EdU$^+$ H9C2 (Figure 11A) and the AUC at 5 days (Figure 11B) compared to the uneducated $M_{(-)}$ secretome.

Similar trends were observed for $M_{(LPS,INF)}$ /F-BMC (Figure 11C,D) while $M_{(IL-4)}$, /F-BMC showed different effects. Indeed, $M_{(IL-4)}$/F-BMC induced proliferation of H9C2 similar to the control (uneducated $M_{(IL-4)}$) and a great reduction in H9C2 spreading (Figure 11E,F). Notably, the uneducated $M_{(IL-4)}$ induced a strong proliferation of H9C2 (Figure 11E,F). This proliferation capacity is maintained when $M_{(IL-4)}$ are educated with F-BMC while H9C2 spreading is reduced.
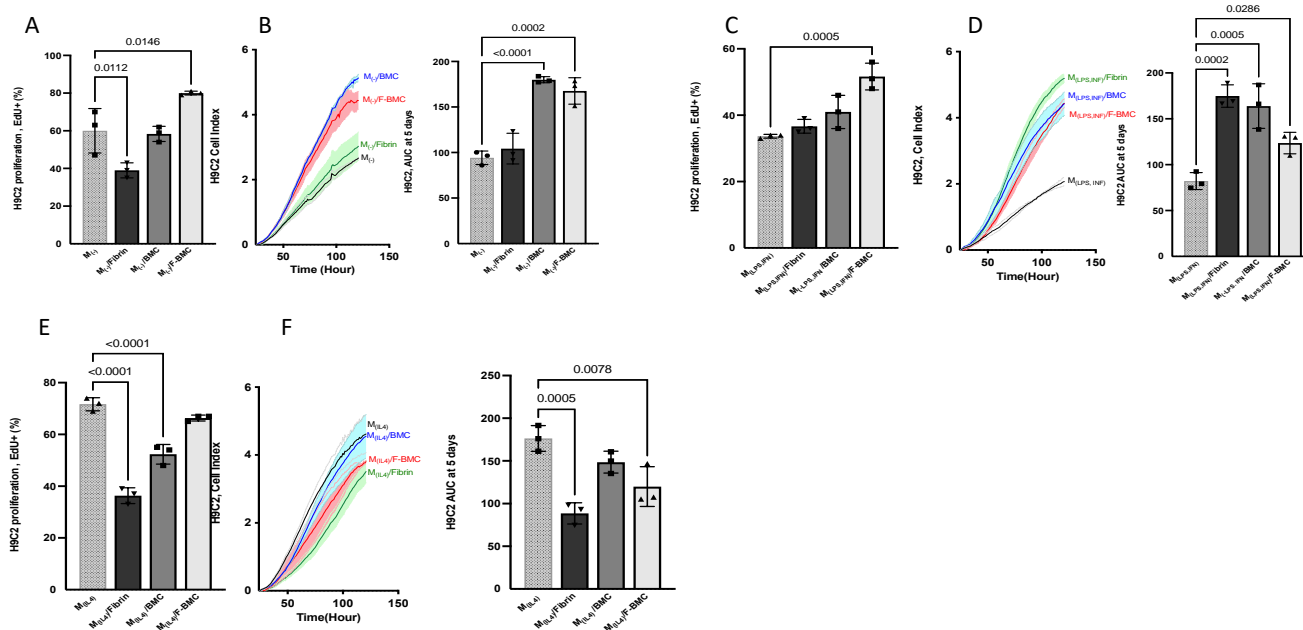
Figure 11. The conditioned media of educated macrophages altered cardiomyoblast H9C2 proliferation rate and spreading. H9C2 were cultured with Cd-media from (**A,B**) educated $M_{(-)}$, (**C,D**) educated $M_{(LPS,IFN)}$ or (**E,F**) educated $M_{(IL-4)}$. Macrophages were cultured with Cd-media from fibrin, BMC or F-BMC, respectively. Cd-medium from uneducated served as the control. H9C2 growth was assessed by (**A,C,E**) EdU incorporation for 48 h and by (**B,D,F**) RTCA: Cell index was measured over 120 h, and the AUC was calculated after five days. The values are shown as mean $\pm$ SD; $n = 3$ biologically independent experiments.

4. Discussion

In the present study, fibrin and BMC were combined to sub-chronically treat the ischemic myocardium. Epicardial implantation reduced MI related loss of cardiac function and prevented fibrotic scar expansion. The therapeutic effect of cell-based therapy is associated with an acute paracrine activation of in situ repair mechanisms [30]. Indeed, secreted mediators are believed to be essential for overcoming post-natal cardiomyocyte cell-cycle arrest, manipulating the microenvironment, stimulating progenitor differentiation and promoting the functional polarization of the non-myocyte cell population.

In addition, following cell-based treatment, the role of the inflammatory response and its resolution has gained increased interest. The presence of macrophages and their role have recently been explored. Vagnozzi et al. [11] demonstrated that CD68$^+$ macrophages were increased within the area of cell injection after three and seven days post-injection; however, their presence vanished after two weeks [11]. The authors suggested that macrophages were associated with the presence of injected cells [11]. It has since been validated that the therapeutic cells survived only a few days after implantation [11,31]. In the present study, MI content of CD68$^+$ and CD206$^+$ macrophages were similar in treated and untreated groups after 4 and 12 weeks. The presence of therapeutic cells is unlikely, and accordingly, the macrophage content is unlikely to be affected at these late stages. Nevertheless, when MSCs were administered together with a slow degrading polycaprolactone matrix, our previous study identified the presence of CD68$^+$ cells four weeks post-treatment [31], suggesting that the chronic presence of macrophages might also be dependent on the lasting presence of the matrix. In the current study, fibrin, as a rapidly degrading matrix, was absent after 4 weeks, which may explain the lack of difference in the macrophage content.

It is reasonable to suggest that the initiation of cardioprotective events leading to scar reduction would occur rapidly after the treatment. Therefore, to understand these potential early events, we investigated in vitro the interaction between the matrix, the therapeutic cells, the macrophages and cells of cardiac origin.

The association of cell and matrix have gained increased interest as a therapeutic product for cardiac repair [32]. The matrix plays a critical role in prolonging cell survival after transplantation [33,34]. Initially used as a scaffold to provide physical substrate for cell survival, the matrix also has multiple effects [35]. The present in vitro study provides evidence of the impacts of the matrix on the therapeutic cells. The fibrin matrix alters the morphology of BMC, their gene expression and protein secretion and fosters their immunomodulatory capacities.

4.1. Impact of Fibrin on BMC and Their Properties

First, we report an effect on BMC morphology and proliferation. BMC is a heterogeneous population of cells with a prevalence of mesenchymal CD90$^+$ cells. It is well established that unfractionated BMCs are composed of monocytes, lymphocytes, hematopoietic stem cells, MSC and progenitors. Accordingly, hybrid properties and inter-cellular crosstalk between all cell types can be expected [36]. We demonstrated that fibrin modified the BMC shape, reduced their spreading and proliferation. In agreement, previous studies demonstrated that MSC showed a modified morphology, a reduced size and a decreased proliferation when cultured with fibrin [37,38]. Furthermore, the fibrin-induced BMC morphological changes were associated with a downregulation of *Icam* and *Vcam1*. These adhesion molecules mediate the interaction between cells and the ECM, and their downregulation could explain the reduced spreading of the cells resulting in a reduced size and rounded shape.

Second, we demonstrated that fibrin induced changes in BMC gene expressions. The most prominent gene upregulation was the expression of *Il1 receptor antagonist* (*IL1ra*) and, to a lesser extent of *Il1b*, while *IL1a* remained unchanged. In normal homeostasis, *IL1ra* counterbalances the effect of *IL1b* and *IL1a* by binding to their common receptor. *IL1ra* has been proposed to be one of the mediators of the therapeutic effect of MSC by antagonizing IL-1 effects and blocking inflammation. Luz-Crawford et al. [39] showed that *IL1ra* secreted by MSC acts on macrophages by inducing a polarization toward the anti-inflammatory phenotype.

Third, we showed an impact of fibrin on the immunomodulatory properties of BMC. The secretomes from both BMC and F-BMC alleviated the gene expression of macrophages and specifically induced a polarization of M$_{(LPS/INF)}$ and M$_{(-)}$ toward alternatively activated macrophage phenotypes. Indeed, BMC and F-BMC educated macrophages increased their expression of anti-inflammatory markers (*Arg1*, *Cd163*, *Cd206*, *Il10*, *Tgfb*) while decreasing pro-inflammatory markers (*Nos2*, *Cd86*, *Il1b*, *Il6*, *Mcp1*, *Tnfa*).

It is well established that MSCs promote the polarization of macrophages to an anti-inflammatory phenotype [40–43]. For instance, co-cultures of MSC and macrophages have shown that MSC induces the conversion of classically activated, pro-inflammatory macrophages to alternatively activated macrophages [26]. Interestingly, our study indicates that the combination of fibrin and BMC further potentiated the anti-inflammatory regulatory capacity of BMC.

Alternatively-activated macrophages mediate the resolution of inflammation by phagocytosis of cellular debris, production of ECM proteins and secretion of cytokines such as IL-10 and TGF-beta [44]. Modulating macrophage phenotypes for salvaging ischemic damage is a promising new therapeutic strategy. Indeed, dampening the inflammatory response using MSC is broadly studied for multiple chronic diseases [45]. As far as MI is concerned, several cell-based treatments have increased CD206$^+$ macrophages. It has been demonstrated that stimulating the anti-inflammatory CD206$^+$ macrophage polarization with cytokines, bioactive drugs or cell treatments improved cardiac tissue repair in MI animal models [46,47]. The current assumption is that a transient CD206$^+$ phenotype effectively clears inflammation and may be advantageous for improved cardiac function and alleviated adverse ventricular remodelling [46]. Nevertheless, a chronic elevation of CD206$^+$ cells could have unwanted consequences due to the fibrotic properties of the alternatively activated macrophage population [48]. Remarkably, a pro- or anti-fibrotic environment may influence the balance between the different macrophage populations identified in MI.

Furthermore, in M$_{(IL-4)}$, *Tnfa* expression was significantly downregulated by F-BMC, and its secretion remained low. Likewise, *Tnfa* secretion by M$_{(LPS, INF)}$ and to a lesser extent by M$_{(−)}$ was significantly reduced in F-BMC educated macrophages. Accordingly, an MSC-conditioned medium has been shown to inhibit the production of TNF-alpha by activated macrophages in vitro through the release of Il-1ra [49]. Therefore, a possible explanation of this reduction is the increase of *Il1ra* in F-BMC.

In addition, F-BMC induced the upregulation of *Tgfb* in all the macrophage subsets. Notably, it has been shown that GREM1 increased the expression of *Tgfb* in hepatic stellate cells and tubular cells [50]. Consistently, the increased GREM1 in the F-BMC secretome could potentially mediate the *Tgfb* elevation.

Fibrin was obtained from fibrinogen and thrombin. Accordingly, the secretome of F-BMC contains more fibrinogen than the one of BMC. Fibrinogen is thought to activate macrophage inflammatory pathways and might affect macrophage polarization in our model. Nevertheless, the pro-inflammatory effect of fibrinogen is inhibited by fibrin [51]. Here, we showed a negligible pro-inflammatory impact of fibrinogen. For instance, the conditioned medium from fibrin alone downregulated the pro-inflammatory related genes and upregulated Cd163 in M$_{(IL-4)}$.

4.2. Cardiomyoblast Fate

F-BMC stimulated the spreading of cardiomyoblasts but not their proliferation. Notably, the proteomics analysis revealed increased Osteopontin (OPN/SSP1) in the secretome of F-BMC. OPN has been associated with cardiac hypertrophy [52]. Therefore, F-BMC induced cardiomyoblast hypertrophy is consistent with OPN level.

Macrophages had an impact on cardiomyoblasts proliferation in a phenotype dependent manner. Uneducated M$_{(IL-4)}$ greatly stimulated H9C2 proliferation while other macrophage subsets did not. Nevertheless, when educated by F-BMC, M$_{(LPS,INF)}$ and M$_{(−)}$ developed a capacity to stimulate cardiomyoblast growth compared to uneducated macrophages. This effect was also promoted by fibrin for M$_{(LPS/INF)}$ and by BMC for M$_{(−)}$. Taken all together, our results suggest that mitogenic properties developed by F-BMC educated M$_{(LPS/INF) and M_{(−)}}$ could be a consequence of their polarization toward an anti-inflammatory phenotype.

Altering cardiomyocyte fate emerged as an effective strategy to compensate for the loss of functional cardiomyocytes following MI. In the present study, we validate in vitro that fibrin and BMC are potential catalyzers of optimal microenvironment conditions to favor the polarization of macrophages. Their role in cardiac repair remains to be investigated. Psarras et al. [7] identified up to seven new cardiac myeloid cell subtypes, including four macrophage populations; their respective role is still not fully understood [6]. However, the crosstalk between cardiac cells and macrophages is essential for cardiac homeostasis [7,11,47,53–55]. In addition to their multifaceted roles in ECM modulation, cardiac electrical conduction and mitochondrial homeostasis [56–58], we reinforce the importance of anti-inflammatory macrophages in regulating proliferative cell fate. The present in vitro results suggest that macrophage plasticity and anti-inflammatory environment are both necessary for modifying cardiomyoblast cell size and proliferation. Nevertheless, further studies need to be undertaken to investigate these effects on other models such as neonatal and adult cardiomyocytes in vitro and also in vivo and validate this present proof-of-concept. Indeed, Vagnozzi et al. [11] showed in vivo that there was no formation of new cardiomyocytes following temporal and regional induction of CCR2 [+] and CX3CR1[+] macrophages. Nevertheless, the understanding of the spatiotemporal role of the macrophage in limiting adverse remodelling is still unclear. Our study suggests that (1) the importance of a scaffold that stimulates an optimal immune response for regeneration is to be considered, and (2) F-BMC may potentially induce an early stimulation of the cardiac reparative process. Further studies are necessary to identify the detailed mechanism in vitro and acute in vivo effects.

4.3. Integrated Concept

Taken all together, as represented in Figure 12, we documented in vitro that first, the F-BMC secretome has crucial effects on macrophage phenotypes: F-BMC induces the polarization of $M_{(-)}$ toward an anti-inflammatory phenotype, a phenotype switch of $M_{(LPS,INF)}$ and the proliferation of $M_{(IL-4)}$. Accordingly, the F-BMC educated macrophages present an anti-inflammatory phenotype and their secretomes favor cardiomyoblast proliferation. Second, the F-BMC secretome promotes cardiomyoblast spreading.
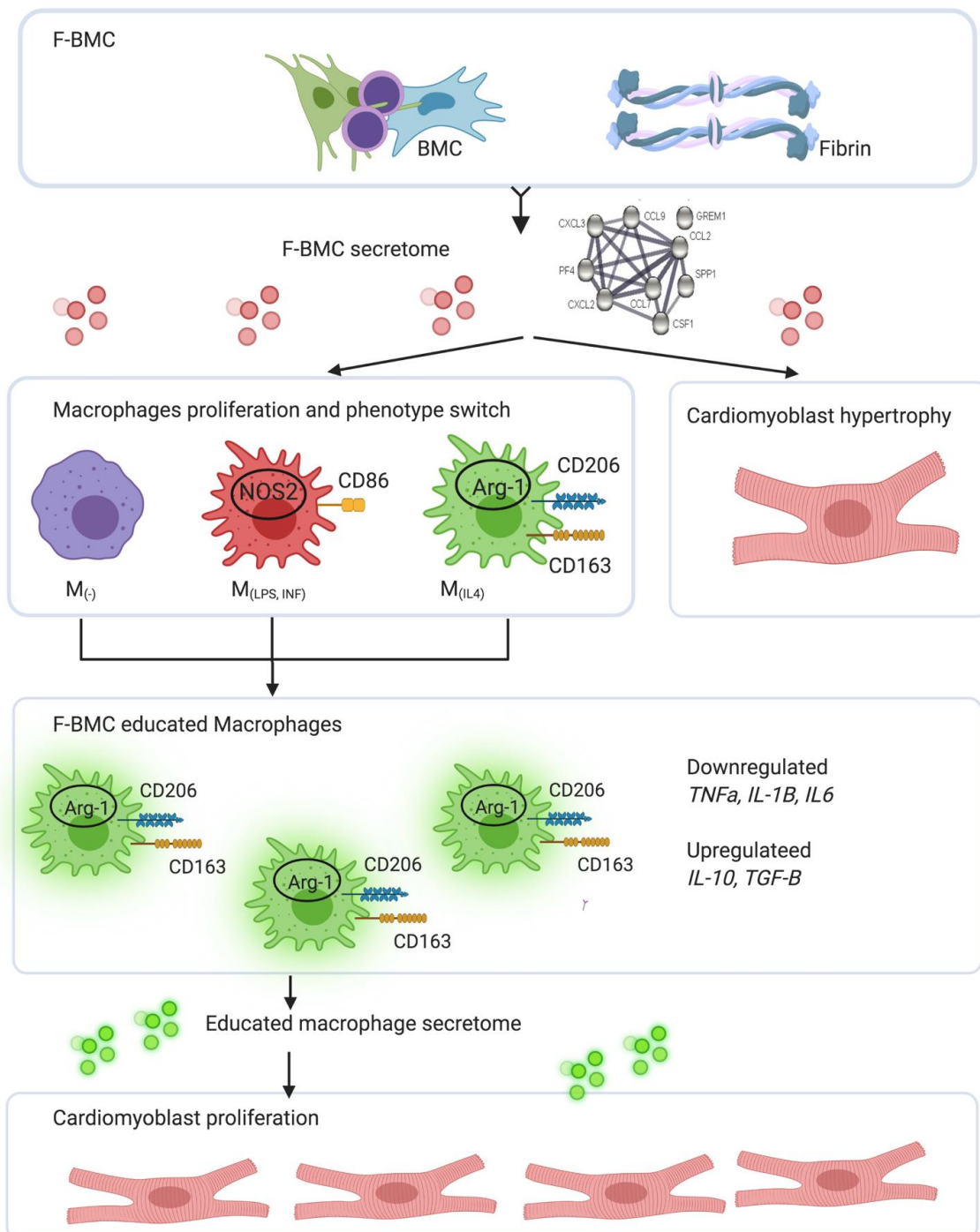

Figure 12. Schematic representation of the integrated concept of the effect of F-BMC on two types of cells: macrophages and cardiomyoblasts. BMC primed with fibrin secreted a specific secretome (analysed by proteomics). The F-BMC secretome induced (1) cardiomyoblast hypertrophy, (2) immunomodulation

leading to phenotype switch in a macrophage subset dependant manner and (3) proliferation of anti-inflammatory macrophages. F-BMC educated macrophages upregulate anti-inflammatory genes and downregulate pro-inflammatory ones. Their secretome induced cardiomyoblast proliferation.

In conclusion, our study provides evidence that in vivo, F-BMC treatment lowered the infarct extent, increased wall thickness and improved cardiac function. In vitro, the F-BMC secretome promoted the growth of anti-inflammatory macrophages, stimulated macrophage plasticity and consequently altered the balance between the pro- and anti-inflammatory macrophage subsets. F-BMC secretome favored the mitogenic properties of anti-inflammatory macrophages promoting cardiac cell growth.

Supplementary Materials: The following supporting information can be downloaded at: https://www.mdpi.com/article/10.3390/biomedicines10030527/s1, Figure S1: CD68+, CD206+ macrophages within the infarcted area and border zone were similar in all groups. Immunostainings for CD206 (A,C) and CD68 (B,D) were performed on paraffin-embedded heart sections. 5 to 6 cross-sections from a systematic sampling of the whole heart were averaged for each animal. Hearts were harvested 4 or 12 weeks post-treatment; Figure S2: Surface markers of BMCs measured by flow cytometry and immunostaining. (A) Histogram represents the flow cytometry results, and the pictures represent the immunostainings of the cells. BMC are a heterogeneous population of cells as indicated by markers from the mesenchymal (CD90, CD29, CD13) and hematopoietic (CD45, CD44, CD68) lineages. The mesenchymal CD90+ cells were most abundant. They form a population of large and spread cells. (B) Quantification of the immunostainings; Figure S3: Comparison of the expression profiles of macrophages cultured in F-BMC, BMC or fibrin conditioned medium; Table S1: Expression proteomic data of conditioned medium of F-BMC and BMC; Table S2: Primers used for real-time PCR analysis.

Author Contributions: I.B. and M.-N.G. designed the experiments; I.B., J.V., A.F., G.A., C.K., M.S. and B.F. conducted the experiments; M.-N.G., I.B. and J.D. analyzed the results; I.B. and M.-N.G. prepared the figures; I.B. and M.-N.G. wrote the main manuscript; M.-N.G. and S.C. provided the resources. The authors reviewed the manuscript. All authors have read and agreed to the published version of the manuscript.

Institutional Review Board Statement: The animal study protocol was approved by the cantonal and Swiss Federal Veterinary Office, Switzerland (FR-2016-41; 23 February 2017).

Informed Consent Statement: Not applicable.

Data Availability Statement: The datasets generated and analyzed during the current study are available from the corresponding author on reasonable request.

Conflicts of Interest: The authors declare no conflict of interest.

References

1. Lavine, K.J.; Pinto, A.R.; Epelman, S.; Kopecky, B.J.; Clemente-Casares, X.; Godwin, J.; Rosenthal, N.; Kovacic, J.C. The Macrophage in Cardiac Homeostasis and Disease: JACC Macrophage in CVD Series (Part 4). *J. Am. Coll. Cardiol.* **2018**, *72*, 2213–2230. [CrossRef] [PubMed]
2. Frangogiannis, N.G. Regulation of the inflammatory response in cardiac repair. *Circ. Res.* **2012**, *110*, 159–173. [CrossRef]
3. Aurora, A.B.; Porrello, E.R.; Tan, W.; Mahmoud, A.I.; Hill, J.A.; Bassel-Duby, R.; Sadek, H.A.; Olson, E.N. Macrophages are required for neonatal heart regeneration. *J. Clin. Investig.* **2014**, *124*, 1382–1392. [CrossRef] [PubMed]
4. Mosser, D.M.; Edwards, J.P. Exploring the full spectrum of macrophage activation. *Nat. Rev. Immunol.* **2008**, *8*, 958–969. [CrossRef] [PubMed]
5. Murray, P.J.; Allen, J.E.; Biswas, S.K.; Fisher, E.A.; Gilroy, D.W.; Goerdt, S.; Gordon, S.; Hamilton, J.A.; Ivashkiv, L.B.; Lawrence, T.; et al. Macrophage activation and polarization: Nomenclature and experimental guidelines. *Immunity* **2014**, *41*, 14–20. [CrossRef]
6. Lafuse, W.P.; Wozniak, D.J.; Rajaram, M.V.S. Role of Cardiac Macrophages on Cardiac Inflammation, Fibrosis and Tissue Repair. *Cells* **2020**, *10*, 51. [CrossRef] [PubMed]

7. Psarras, S.; Beis, D.; Nikouli, S.; Tsikitis, M.; Capetanaki, Y. Three in a Box: Understanding Cardiomyocyte, Fibroblast, and Innate Immune Cell Interactions to Orchestrate Cardiac Repair Processes. *Front. Cardiovasc. Med.* **2019**, *6*, 32. [CrossRef]

8. Moskalik, A.; Niderla-Bielinska, J.; Ratajska, A. Multiple roles of cardiac macrophages in heart homeostasis and failure. *Heart Fail. Rev.* **2021**. [CrossRef]

9. Carotenuto, F.; Teodori, L.; Maccari, A.M.; Delbono, L.; Orlando, G.; Di Nardo, P. Turning regenerative technologies into treatment to repair myocardial injuries. *J. Cell. Mol. Med.* **2020**, *24*, 2704–2716. [CrossRef]

10. Zhang, S.; Chen, R.; Chakrabarti, S.; Su, Z. Resident macrophages as potential therapeutic targets for cardiac ageing and injury. *Clin. Transl. Immunol.* **2020**, *9*, e1167. [CrossRef]

11. Vagnozzi, R.J.; Maillet, M.; Sargent, M.A.; Khalil, H.; Johansen, A.K.Z.; Schwanekamp, J.A.; York, A.J.; Huang, V.; Nahrendorf, M.; Sadayappan, S.; et al. An acute immune response underlies the benefit of cardiac stem cell therapy. *Nature* **2020**, *577*, 405–409. [CrossRef] [PubMed]

12. Wagner, M.J.; Khan, M.; Mohsin, S. Healing the Broken Heart; The Immunomodulatory Effects of Stem Cell Therapy. *Front. Immunol.* **2020**, *11*, 639. [CrossRef] [PubMed]

13. Zhang, Z.; Tian, H.; Yang, C.; Liu, J.; Zhang, H.; Wang, J.; Hu, S.; Sun, Z.; He, K.; Chen, G. Mesenchymal Stem Cells Promote the Resolution of Cardiac Inflammation After Ischemia Reperfusion Via Enhancing Efferocytosis of Neutrophils. *J. Am. Heart Assoc.* **2020**, *9*, e014397. [CrossRef]

14. Podaru, M.N.; Fields, L.; Kainuma, S.; Ichihara, Y.; Hussain, M.; Ito, T.; Kobayashi, K.; Mathur, A.; D'Acquisto, F.; Lewis-McDougall, F.; et al. Reparative macrophage transplantation for myocardial repair: A refinement of bone marrow mononuclear cell-based therapy. *Basic Res. Cardiol.* **2019**, *114*, 34. [CrossRef] [PubMed]

15. Carty, F.; Mahon, B.P.; English, K. The influence of macrophages on mesenchymal stromal cell therapy: Passive or aggressive agents? *Clin. Exp. Immunol.* **2017**, *188*, 1–11. [CrossRef] [PubMed]

16. Khodayari, S.; Khodayari, H.; Amiri, A.Z.; Eslami, M.; Farhud, D.; Hescheler, J.; Nayernia, K. Inflammatory Microenvironment of Acute Myocardial Infarction Prevents Regeneration of Heart with Stem Cells Therapy. *Cell Physiol. Biochem.* **2019**, *53*, 887–909.

17. Deng, S.; Zhou, X.; Ge, Z.; Song, Y.; Wang, H.; Liu, X.; Zhang, D. Exosomes from adipose-derived mesenchymal stem cells ameliorate cardiac damage after myocardial infarction by activating S1P/SK1/S1PR1 signaling and promoting macrophage M2 polarization. *Int. J. Biochem. Cell. Biol.* **2019**, *114*, 105564. [CrossRef] [PubMed]

18. Wang, Y.; Han, B.; Wang, Y.; Wang, C.; Zhang, H.; Xue, J.; Wang, X.; Niu, T.; Niu, Z.; Chen, Y. Mesenchymal stem cell-secreted extracellular vesicles carrying TGF-beta1 upregulate miR-132 and promote mouse M2 macrophage polarization. *J. Cell. Mol. Med.* **2020**, *24*, 12750–12764. [CrossRef]

19. Madonna, R.; Van Laake, L.W.; Botker, H.E.; Davidson, S.M.; De Caterina, R.; Engel, F.B.; Eschenhagen, T.; Fernandez-Aviles, F.; Hausenloy, D.J.; Hulot, J.S.; et al. ESC Working Group on Cellular Biology of the Heart: Position paper for Cardiovascular Research: Tissue engineering strategies combined with cell therapies for cardiac repair in ischaemic heart disease and heart failure. *Cardiovasc. Res.* **2019**, *115*, 488–500. [CrossRef]

20. Valles, G.; Bensiamar, F.; Crespo, L.; Arruebo, M.; Vilaboa, N.; Saldana, L. Topographical cues regulate the crosstalk between MSCs and macrophages. *Biomaterials* **2015**, *37*, 124–133. [CrossRef]

21. Chen, Y.; Shu, Z.; Qian, K.; Wang, J.; Zhu, H. Harnessing the Properties of Biomaterial to Enhance the Immunomodulation of Mesenchymal Stem Cells. *Tissue Eng. Part B Rev.* **2019**, *25*, 492–499. [CrossRef] [PubMed]

22. Roura, S.; Galvez-Monton, C.; Bayes-Genis, A. Fibrin, the preferred scaffold for cell transplantation after myocardial infarction? An old molecule with a new life. *J. Tissue Eng. Regen. Med.* **2017**, *11*, 2304–2313. [CrossRef] [PubMed]

23. Frobert, A.; Valentin, J.; Cook, S.; Lopes-Vicente, J.; Giraud, M.N. Cell-based therapy for heart failure in rat: Double thoracotomy for myocardial infarction and epicardial implantation of cells and biomatrix. *J. Vis. Exp.* **2014**, *91*, 51390. [CrossRef] [PubMed]

24. Frobert, A.; Valentin, J.; Magnin, J.L.; Riedo, E.; Cook, S.; Giraud, M.N. Prognostic Value of Troponin I for Infarct Size to Improve Preclinical Myocardial Infarction Small Animal Models. *Front. Physiol.* **2015**, *6*, 353. [CrossRef]

25. Valentin, J.; Frobert, A.; Ajalbert, G.; Cook, S.; Giraud, M.N. Histological Quantification of Chronic Myocardial Infarct in Rats. *J. Vis. Exp.* **2016**, *118*, e54914. [CrossRef]

26. Vasandan, A.B.; Jahnavi, S.; Shashank, C.; Prasad, P.; Kumar, A.; Prasanna, S.J. Human Mesenchymal stem cells program macrophage plasticity by altering their metabolic status via a PGE2-dependent mechanism. *Sci. Rep.* **2016**, *6*, 38308. [CrossRef]

27. Roshan Moniri, M.; Young, A.; Reinheimer, K.; Rayat, J.; Dai, L.J.; Warnock, G.L. Dynamic assessment of cell viability, proliferation and migration using real time cell analyzer system (RTCA). *Cytotechnology* **2015**, *67*, 379–386. [CrossRef]

28. Cox, J.; Hein, M.Y.; Luber, C.A.; Paron, I.; Nagaraj, N.; Mann, M. Accurate proteome-wide label-free quantification by delayed normalization and maximal peptide ratio extraction, termed MaxLFQ. *Mol. Cell Proteom.* **2014**, *13*, 2513–2526. [CrossRef]

29. Szklarczyk, D.; Gable, A.L.; Lyon, D.; Junge, A.; Wyder, S.; Huerta-Cepas, J.; Simonovic, M.; Doncheva, N.T.; Morris, J.H.; Bork, P.; et al. STRING v11: Protein-protein association networks with increased coverage, supporting functional discovery in genome-wide experimental datasets. *Nucleic. Acids. Res.* **2019**, *47*, D607–D613. [CrossRef]

30. Rafatian, G.; Davis, D.R. Concise Review: Heart-Derived Cell Therapy 2.0: Paracrine Strategies to Increase Therapeutic Repair of Injured Myocardium. *Stem Cells* **2018**, *36*, 1794–1803. [CrossRef]

31. Guex, A.G.; Frobert, A.; Valentin, J.; Fortunato, G.; Hegemann, D.; Cook, S.; Carrel, T.P.; Tevaearai, H.T.; Giraud, M.N. Plasma-functionalized electrospun matrix for biograft development and cardiac function stabilization. *Acta Biomater.* **2014**, *10*, 2996–3006. [CrossRef] [PubMed]

32. Vaka, R.; Davis, D.R. State-of-play for cellular therapies in cardiac repair and regeneration. *Stem Cells* **2021**, *39*, 1579–1588. [CrossRef] [PubMed]

33. Kanda, P.; Davis, D.R. Cellular mechanisms underlying cardiac engraftment of stem cells. *Expert. Opin. Biol. Ther.* **2017**, *17*, 1127–1143. [CrossRef] [PubMed]

34. Xiong, Q.; Hill, K.L.; Li, Q.; Suntharalingam, P.; Mansoor, A.; Wang, X.; Jameel, M.N.; Zhang, P.; Swingen, C.; Kaufman, D.S.; et al. A fibrin patch-based enhanced delivery of human embryonic stem cell-derived vascular cell transplantation in a porcine model of postinfarction left ventricular remodeling. *Stem Cells* **2011**, *29*, 367–375. [CrossRef] [PubMed]

35. Vegas, A.J.; Veiseh, O.; Doloff, J.C.; Ma, M.; Tam, H.H.; Bratlie, K.; Li, J.; Bader, A.R.; Langan, E.; Olejnik, K.; et al. Combinatorial hydrogel library enables identification of materials that mitigate the foreign body response in primates. *Nat. Biotechnol.* **2016**, *34*, 345–352. [CrossRef]

36. Stevens, H.Y.; Bowles, A.C.; Yeago, C.; Roy, K. Molecular Crosstalk Between Macrophages and Mesenchymal Stromal Cells. *Front. Cell. Dev. Biol.* **2020**, *8*, 600160. [CrossRef]

37. Haasper, C.; Breitbart, A.; Hankemeier, S.; Wehmeier, M.; Hesse, E.; Citak, M.; Krettek, C.; Zeichen, J.; Jagodzinski, M. Influence of fibrin glue on proliferation and differentiation of human bone marrow stromal cells seeded on a biologic 3-dimensional matrix. *Technol. Health Care* **2008**, *16*, 93–101. [CrossRef]

38. Stolzing, A.; Colley, H.; Scutt, A. Effect of age and diabetes on the response of mesenchymal progenitor cells to fibrin matrices. *Int. J. Biomater.* **2011**, *2011*, 378034. [CrossRef]

39. Luz-Crawford, P.; Djouad, F.; Toupet, K.; Bony, C.; Franquesa, M.; Hoogduijn, M.J.; Jorgensen, C.; Noel, D. Mesenchymal Stem Cell-Derived Interleukin 1 Receptor Antagonist Promotes Macrophage Polarization and Inhibits B Cell Differentiation. *Stem Cells* **2016**, *34*, 483–492. [CrossRef]

40. Melief, S.M.; Geutskens, S.B.; Fibbe, W.E.; Roelofs, H. Multipotent stromal cells skew monocytes towards an anti-inflammatory interleukin-10-producing phenotype by production of interleukin-6. *Haematologica* **2013**, *98*, 888–895. [CrossRef]

41. Chiossone, L.; Conte, R.; Spaggiari, G.M.; Serra, M.; Romei, C.; Bellora, F.; Becchetti, F.; Andaloro, A.; Moretta, L.; Bottino, C. Mesenchymal Stromal Cells Induce Peculiar Alternatively Activated Macrophages Capable of Dampening Both Innate and Adaptive Immune Responses. *Stem Cells* **2016**, *34*, 1909–1921. [CrossRef] [PubMed]

42. Maggini, J.; Mirkin, G.; Bognanni, I.; Holmberg, J.; Piazzon, I.M.; Nepomnaschy, I.; Costa, H.; Canones, C.; Raiden, S.; Vermeulen, M.; et al. Mouse bone marrow-derived mesenchymal stromal cells turn activated macrophages into a regulatory-like profile. *PLoS ONE* **2010**, *5*, e9252. [CrossRef] [PubMed]

43. Kim, J.; Shapiro, L.; Flynn, A. The clinical application of mesenchymal stem cells and cardiac stem cells as a therapy for cardiovascular disease. *Pharmacol. Ther.* **2015**, *151*, 8–15. [CrossRef] [PubMed]

44. Shapouri-Moghaddam, A.; Mohammadian, S.; Vazini, H.; Taghadosi, M.; Esmaeili, S.A.; Mardani, F.; Seifi, B.; Mohammadi, A.; Afshari, J.T.; Sahebkar, A. Macrophage plasticity, polarization, and function in health and disease. *J. Cell Physiol.* **2018**, *233*, 6425–6440. [CrossRef] [PubMed]

45. Peng, H.; Shindo, K.; Donahue, R.R.; Abdel-Latif, A. Cardiac Cell Therapy: Insights into the Mechanisms of Tissue Repair. *Int. J. Mol. Sci.* **2021**, *22*, 1201. [CrossRef]

46. Kim, Y.; Nurakhayev, S.; Nurkesh, A.; Zharkinbekov, Z.; Saparov, A. Macrophage Polarization in Cardiac Tissue Repair Following Myocardial Infarction. *Int. J. Mol. Sci.* **2021**, *22*, 2715. [CrossRef]

47. Hobby, A.R.H.; Berretta, R.M.; Eaton, D.M.; Kubo, H.; Feldsott, E.; Yang, Y.; Headrick, A.L.; Koch, K.A.; Rubino, M.; Kurian, J.; et al. Cortical bone stem cells modify cardiac inflammation after myocardial infarction by inducing a novel macrophage phenotype. *Am. J. Physiol. Heart Circ. Physiol.* **2021**, *321*, H684–H701. [CrossRef]

48. Braga, T.T.; Agudelo, J.S.; Camara, N.O. Macrophages During the Fibrotic Process: M2 as Friend and Foe. *Front. Immunol.* **2015**, *6*, 602. [CrossRef]

49. Ortiz, L.A.; Dutreil, M.; Fattman, C.; Pandey, A.C.; Torres, G.; Go, K.; Phinney, D.G. Interleukin 1 receptor antagonist mediates the antiinflammatory and antifibrotic effect of mesenchymal stem cells during lung injury. *Proc. Natl. Acad. Sci. USA* **2007**, *104*, 11002–11007. [CrossRef]

50. Zhang, Y.Q.; Wan, L.Y.; He, X.M.; Ni, Y.R.; Wang, C.; Liu, C.B.; Wu, J.F. Gremlin1 Accelerates Hepatic Stellate Cell Activation Through Upregulation of TGF-Beta Expression. *DNA Cell. Biol.* **2017**, *36*, 603–610. [CrossRef]

51. Hsieh, J.Y.; Smith, T.D.; Meli, V.S.; Tran, T.N.; Botvinick, E.L.; Liu, W.F. Differential regulation of macrophage inflammatory activation by fibrin and fibrinogen. *Acta Biomater.* **2017**, *47*, 14–24. [CrossRef] [PubMed]

52. Martins, C.M.; de Azevedo Queiroz, I.O.; Ervolino, E.; Cintra, L.T.A.; Gomes-Filho, J.E. RUNX-2, OPN and OCN expression induced by grey and white mineral trioxide aggregate in normal and hypertensive rats. *Int. Endod. J.* **2018**, *51*, 641–648. [CrossRef] [PubMed]

53. Bollini, S.; Emanueli, C. To serve and protect: A new heart patrolling and recycling role for macrophages. *Cardiovasc. Res.* **2021**, *117*, e17–e20. [CrossRef] [PubMed]

54. Roy, S.; Spinali, K.; Schmuck, E.G.; Kink, J.A.; Hematti, P.; Raval, A.N. Cardiac fibroblast derived matrix-educated macrophages express VEGF and IL-6, and recruit mesenchymal stromal cells. *J. Immunol. Regen. Med.* **2020**, *10*, 100033. [CrossRef] [PubMed]

55. Hitscherich, P.; Lee, E.J. Crosstalk Between Cardiac Cells and Macrophages Postmyocardial Infarction: Insights from In Vitro Studies. *Tissue Eng. Part B Rev.* **2021**, *27*, 475–485. [CrossRef]

56. Alvarez-Argote, S.; O'Meara, C.C. The Evolving Roles of Cardiac Macrophages in Homeostasis, Regeneration, and Repair. *Int. J. Mol. Sci.* **2021**, *22*, 7923. [CrossRef]

57. Vagnozzi, R.J.; Molkentin, J.D. Resident macrophages keep mitochondria running in the heart. *Cell Res.* **2020**, *30*, 1057–1058. [CrossRef]

58. Bartelt, A.; Weber, C. Mitochondrial Ejection for Cardiac Protection: The Macrophage Connection. *Cell Metab.* **2020**, *32*, 512–513. [CrossRef]